Effects of low frequency electromagnetic casting on solidification macrostructure of GH4742 superalloy

Liang Zhang[1], *Lei Wang[1], Yang Liu[1], Xiu Song[1], Teng Yu[2], and Ran Duan[3]

1. Key Laboratory for Anisotropy and Texture of Materials, Ministry of Education, School of Materials Science and Engineering, Northeastern University, Shenyang 110819, China

2. High Temperature Materials Division, Fushun Special Steel Co., Ltd., Fushun 113001, Liaoning, China

3. Gaona Aero Material Co., Ltd., Beijing 100081, China

Abstract: The low frequency electromagnetic casting (LFEC) was used to prevent hot cracking during the solidification process of GH4742 superalloy ingot. The effects of LFEC on the solidification macrostructure of the ingot were investigated through experiments and simulation. The results show that the average grain size decreases after application of LFEC. At the same time, the fraction of equiaxed grains increases compared with the ingots that without LFEC. In addition, the average grain size decreases and the fraction of equiaxed grains increases with increasing the current frequency. When the current frequency increases from 5 Hz to 20 Hz, the average grain size decreases from 5.39 mm to 4.74 mm, and the fraction of equiaxed grains increases from 41.21% to 55.24%. The distribution of Lorentz force, melt flow field and temperature field in the melt was simulated using COMSOL Multiphysics software. It is found that the Lorentz force increases and the forced convection is enhanced with increasing the current frequency, thus the melt flow velocity and heat transfer in the melt are promoted. It can facilitate the heterogenous nucleation in the melt, resulting in grain refinement, and further preventing hot cracking of large size ingots.

Keywords: low frequency electromagnetic casting; superalloy; solidification; hot cracking; grain refinement

CLC numbers: TG146.1⁺5 **Document code:** A **Article ID:** 1672-6421(2025)02-195-10

1 Introduction

As one of the typical precipitation-strengthening nickel-based superalloys, GH4742 alloy has excellent combination of mechanical properties and high corrosion resistance at high temperatures [1]. It has been commonly used in aerospace engines and gas turbines [2]. With aero-engines become larger and the development of advanced equipment manufacturing industry, the demand for large size master superalloy ingots becomes more urgent. Currently, the most common melting process for superalloys is combination of vacuum induction melting (VIM), electroslag remelting (ESR), and vacuum arc remelting (VAR). VIM is the first melting process to produce superalloy ingots, and it has several advantages such as precise control of the alloy composition, high alloy purity and prevention of oxidation. However, it also shows some shortcomings, such as coarse grains and serious element segregation, which can often lead to hot cracking in large size VIM superalloy ingots [3]. If the VIM ingot contains cracks, metallurgical defects such as freckle or white spot are usually induced in the VAR or ESR ingots. It will seriously reduce the quality and yield of superalloy products. Therefore, manufacturing crack-free VIM superalloy ingots is the key foundation for high quality of superalloy products.

There are several factors influencing the hot cracking behavior of ingots, especially grain size and the fraction of equiaxed grains in the microstructure. It is widely acknowledged that hot cracking tendency decreases with grain refinement [4,5]. For example, Li et al. [6] found that hot cracking of the Al-Cu alloy can be decreased through grain refinement. Lin et al. [7] found that hot tearing susceptibility decreased with grain refinement

***Lei Wang**

Professor. His research interests are focused on the strengthening and toughening of advanced materials with microstructural control, and the mechanical behavior of materials under dynamic loading and other environments. To date, he has published more than 380 papers and 10 books.

E-mail: wanglei@mail.neu.edu.cn

Received: 2024-05-22; Revised: 2024-06-20; Accepted: 2024-09-09

in the aluminum alloy. Fine equiaxed grains not only increase the strength of alloy, but also improve the ability of liquid feeding during solidification. Therefore, grain refinement is an effective method for reducing the hot cracking tendency of ingots. In order to obtain fine grains during solidification, various methods have been used, such as adding grain refiner, chemical refinement, rapid solidification, and applying an external physical field.

At present, adding grain refiner is widely used to produce a fine and uniform microstructure for aluminum alloy [8,9]. However, it is not applicable for superalloys due to pollution of the melt. Moreover, rapid solidification is not suitable for manufacturing large size superalloy ingots. While, applying an external physical field is a green, easy to control and efficient method to achieve grain refinement for superalloy ingots, and most importantly, it does not pollute the melt. The effects of external physical fields such as mechanical vibration [10,11], ultrasonic processing [12,13], permanent magnet stirring [14,15], electromagnetic stirring [16,17], low frequency electromagnetic casting [18,19] on microstructure have been studied. Forced convection can be induced through the application of external physical fields, which in turn can promote the fragmentation of dendrites, facilitating the columnar to equiaxed transition (CET) and results in grain refinement. In this way, fine and uniform grains and good surface quality can be obtained.

Compared with other external physical fields, low frequency electromagnetic field is easy to be controlled and has a high instantaneous energy. Grain refinement can be achieved by using a low frequency electromagnetic field through adjusting current density and frequency. More recently, the low frequency electromagnetic casting (LFEC) has been applied to aluminum and magnesium alloys [20,21]. However, the effect of LFEC on the solidification microstructure of superalloys has not been reported yet. Therefore, it is essential to investigate the grain refinement and CET mechanism of LFEC for the GH4742 superalloy.

In the present study, the effects of LFEC on solidification macrostructure of GH4742 superalloy ingots were investigated through both experiment and numerical simulation. Under the electromagnetic field, the solidification is a transient and complex process. Moreover, the melt is opaque and at a very high temperature. Therefore, it is impossible to obtain the real Lorentz force field, temperature field, and the melt flow field during the solidification directly through experimental measurements. Thus, numerical simulation using COMSOL Multiphysics software was performed. The mechanism of grain refinement and CET in GH4742 ingots through applying LFEC was also revealed. This study will provide an important reference and theoretical basis for reducing hot cracking tendency of superalloy ingots by grain refinement of LFEC.

2 Experimental procedure and numerical simulation

2.1 Experimental facility

Figure 1 shows the schematic diagram of the LFEC facility used for the present study, which consists of a low frequency electromagnetic (LFE) control system and a casting unit including an induction coil, a water-cooling system, a refractory mold and a firebrick. The electromagnetic field is generated by 360 turns induction coil wound around the mold.

2.2 Solidification experiment

The nominal chemical compositions (wt.%) of GH4742 superalloy used in the present study were 0.065 C, 14 Cr, 10 Co, 5 Mo, 2.6 Al, 2.6 Ti, 2.6 Nb, and balance Ni. The alloy was melted with a VIM furnace (ZG 0.025). Then, the alloy melt was heated to 1,823 K, held for 5 min, and then poured into a cylindrical mold with an inner diameter of 60 mm and a height of 195 mm. The LFEC equipment was set up with a mold in side, which switched on before pouring the molten melt, and kept until the solidification process finished. The current density was set at 100 A, with current frequencies of 5 Hz, 10 Hz, and 20 Hz, respectively. For comparison, an ingot was also cast using the same process without the electromagnetic field.

2.3 Macrostructure observation

The ingots were cut along the longitudinal section, and then ground, polished and etched using a solution of 150 g $CuSO_4$+ 35 mL H_2SO_4+500 mL HCl to observe the as-cast macrostructure. The average grain size and the fraction of equiaxed grains were measured using Nano Measurer software and ImageJ software, respectively.

2.4 Numerical simulation

Numerical simulation was preformed using COMSOL Multiphysics software to investigate effects of LFEC on the macrostructure of GH4742 superalloy ingots. The Lorentz force field, melt flow field, and temperature field were calculated. In the present study, since both the mold and the induction coil were two-dimensional axisymmetric structures, the numerical simulation model was simplified to a two-dimensional axisymmetric geometry model.

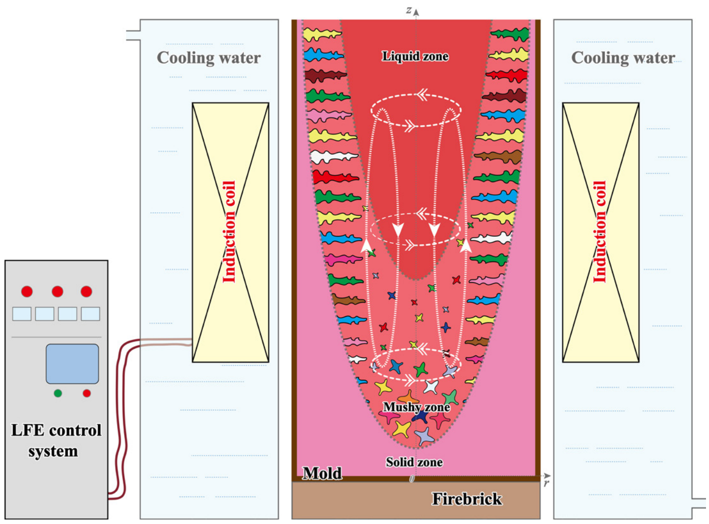

Fig. 1: Schematic diagram of the LFEC facility

The numerical simulation process employed a series of governing equations with the application of the low frequency electromagnetic field [22,23]. During the LFEC process, the distribution of the electromagnetic field can be solved by using Maxwell's equations. These equations can be simplified as:

$$\nabla \times \boldsymbol{E} = -\frac{\partial \boldsymbol{B}}{\partial t} \tag{1}$$

$$\nabla \times \boldsymbol{B} = \sigma \boldsymbol{E} \tag{2}$$

$$\nabla \cdot \boldsymbol{E} = 0 \tag{3}$$

$$\nabla \cdot \boldsymbol{B} = 0 \tag{4}$$

where $\boldsymbol{E}$ is the electric field intensity, $\boldsymbol{B}$ is the magnetic flux density, t is the time and σ is the electric conductivity.

The induced current $\boldsymbol{J}$ can be solved with Ohm's law, which written as:

$$\boldsymbol{J} = \sigma \boldsymbol{E} \tag{5}$$

The Lorentz force in the melt can be given as:

$$\boldsymbol{F} = \boldsymbol{J} \times \boldsymbol{B} \tag{6}$$

Then, the governing equations for flow field and temperature field are as follows:

Conservation equation of mass:

$$\frac{\partial \rho}{\partial t} + \nabla \cdot (\rho \boldsymbol{U}) = 0 \tag{7}$$

Conservation equation of momentum:

$$\frac{\partial(\rho \boldsymbol{U})}{\partial t} + \nabla \cdot (\rho \boldsymbol{U}\boldsymbol{U}) = \nabla \cdot (\mu_{\mathrm{eff}} \nabla \boldsymbol{U}) - \nabla P - A_{\mathrm{mush}} \frac{(1-f_{\mathrm{l}})^2}{f_{\mathrm{l}}^3 + \chi}(\boldsymbol{U} - \boldsymbol{U}_{\mathrm{s}}) + \rho g \beta (T - T_{\mathrm{ref}}) + \boldsymbol{J} \times \boldsymbol{B} \tag{8}$$

Conservation equation of energy:

$$\frac{\partial(\rho T)}{\partial t} + \nabla \cdot (\rho \boldsymbol{U} T) = \nabla \cdot \left(\frac{k}{C_{\mathrm{p}}} \nabla T\right) \tag{9}$$

where ρ is the density; $\boldsymbol{U}$ is the flow velocity; μ_{eff} is the effective viscosity, expressed as $\mu_{\mathrm{eff}}=\mu_{\mathrm{t}}+\mu_{\mathrm{l}}$, ($\mu_{\mathrm{t}}$ is the turbulent viscosity, and μ_{l} is the laminar viscosity); P is the pressure; A_{mush} is the mushy zone constant, χ is a very small constant used to prevent division by zero [24]; $\boldsymbol{U}_{\mathrm{s}}$ is the velocity of the solid phase; g is the gravity; β is the volume expansion coefficient; T is the temperature, T_{ref} is the reference temperature; C_{p} is the specific heat of the alloy, and k is the thermal conductivity.

The liquid fraction (f_{l}) and solid fraction (f_{s}) can be written as:

$$f_{\mathrm{l}} = \begin{cases} 0,\ T \le T_{\mathrm{s}} \\ 1 - \dfrac{1}{1-k_{\mathrm{p}}} \cdot \dfrac{T_{\mathrm{l}} - T}{T_{\mathrm{m}} - T},\ T_{\mathrm{s}} < T < T_{\mathrm{l}} \\ 1,\ T \ge T_{\mathrm{l}} \end{cases} \tag{10}$$

$$f_{\mathrm{s}} = 1 - f_{\mathrm{l}} \tag{11}$$

where T_{s} is the solidus temperature, T_{l} is the liquids temperature, T_{m} is melting point temperature of the pure nickel metal, and k_{p} is the solute partition coefficient.

Table 1 lists the physical properties of GH4742 superalloy. The initial melt temperature was set at 1,750 K.

For simplifying the mathematical model, some assumptions were required as follows [26]:

(1) The GH4742 superalloy molten melt was treated as the incompressible fluid.

(2) The filling process of the molten melt was not taken into account.

(3) Because the Joule heat was much smaller than the heat of the melt, it was not considered in this model.

(4) The displacement current was not considered.

(5) Because the magnetic Reynolds number was significantly smaller than 1, the effect of the melt flow field on the magnetic field distribution was neglected.

Table 1: Physical properties of GH4742 superalloy [25]

Parameter	Value
Electric conductivity, σ	7.4×10^5 S·m^{-1}
Density, ρ	8,230 kg·m^{-3}
Solidus temperature, T_{s}	1,405 K
Liquids temperature, T_{l}	1,622 K
Melting point temperature, T_{m}	1,728 K
Specific heat, C_{p}	As shown in Fig. 2
Latent heat, L	2.3×10^5 J·kg^{-1}
Volume expansion coefficient, β	3.1×10^{-5} K^{-1}
Thermal conductivity, k	29.5 W·(m·K)$^{-1}$

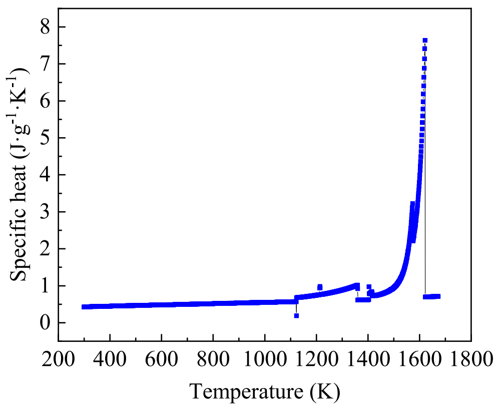

Fig. 2: Specific heat of GH4742 superalloy

3 Results

3.1 Solidification macrostructure

The solidification macrostructures of the GH4742 superalloy ingots without and with the LFEC of different current frequencies are shown in Fig. 3. It is clear that the macrostructure consists of columnar grains at the edge and equiaxed grains at the center of ingots under both conditions. The macrostructure without LFEC is shown in Fig. 3(a). In the upper part of the ingot, there are mainly larger columnar grains grown perpendicular to the mold surface, which is the heat transfer direction. In the lower part of the ingot, there are only a few coarse equiaxed grains. It is clearly observed from Figs. 3(b–d) that the grain size becomes smaller with the LFEC applied, and the equiaxed grains become smaller with increasing the current frequency. When the current frequency is increased to 20 Hz, the macrostructure exhibits completely fine equiaxed grains in the ingot center, and only a few columnar grains at the edge. It is noted that significant CET occurs when the low frequency electromagnetic field is applied, and it becomes more pronounced with increasing the current frequency.

The statistical results of the average equiaxed grain size and the fraction of equiaxed grains are shown in Figs. 4(a) and (b), respectively. The average equiaxed grain size reduces and the fraction of equiaxed grains increases after application of LFEC. Additionally, the average equiaxed grain size gradually decreases and the fraction of equiaxed grains increases with increasing the current frequency. As shown in Fig. 4(a), the average equiaxed grain size decreases from 5.39 mm (at the current frequency of 5 Hz) to 4.74 mm (at the current frequency of 20 Hz). Figure 4(b) illustrates that the fraction of equiaxed grains increases from 41.21% (at the current frequency of 5 Hz) to 55.24% (at the current frequency of 20 Hz).

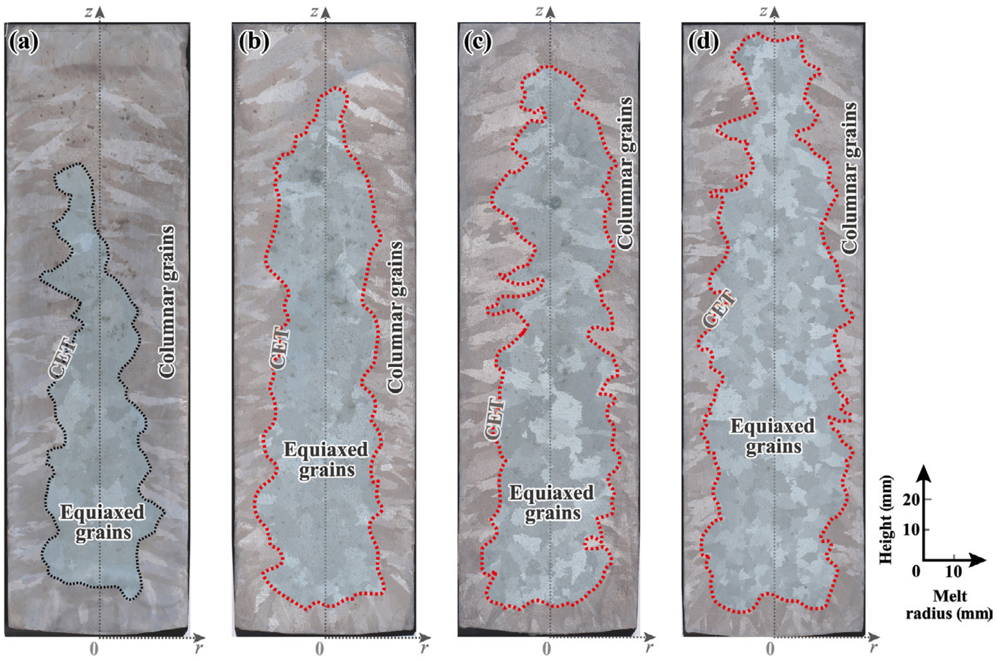

Fig. 3: Solidification macrostructure of GH4742 superalloy ingots: (a) without LFEC; (b) 5 Hz; (c) 10 Hz; (d) 20 Hz

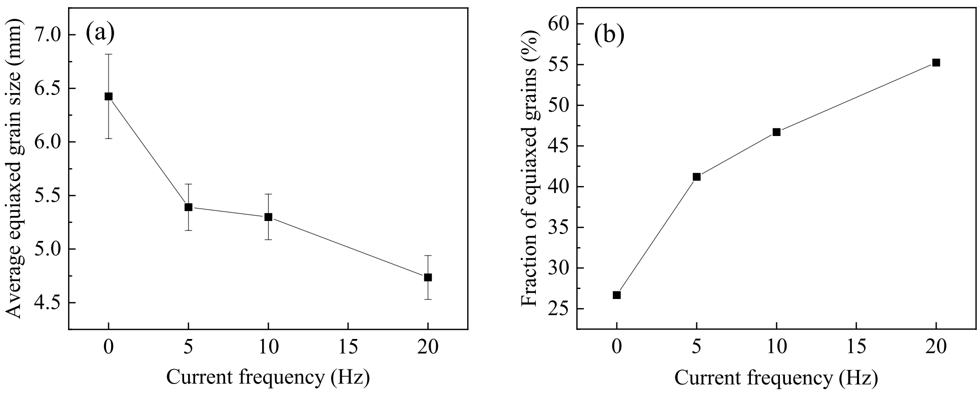

Fig. 4: Average equiaxed grain size (a) and fraction of equiaxed grains (b)

3.2 Lorentz force field

The distributions of Lorentz force in the melt with different current frequencies are shown in Fig. 5. It is evident that the Lorentz force mainly concentrates near the melt surface and increases significantly with increasing the current frequency. While, Lorentz force decreases from the edge to the center of the ingot due to skin effect.

3.3 Melt flow field

The Lorentz force generated by LFEC is the driving force for the melt flow. Figure 6 shows the melt flow field with different current frequencies at 15 s. The variation trend of the melt velocity is consistent with that of the Lorentz force, i.e., the melt velocity increases with increasing the current frequency. In addition, the melt velocity is higher at the melt center than

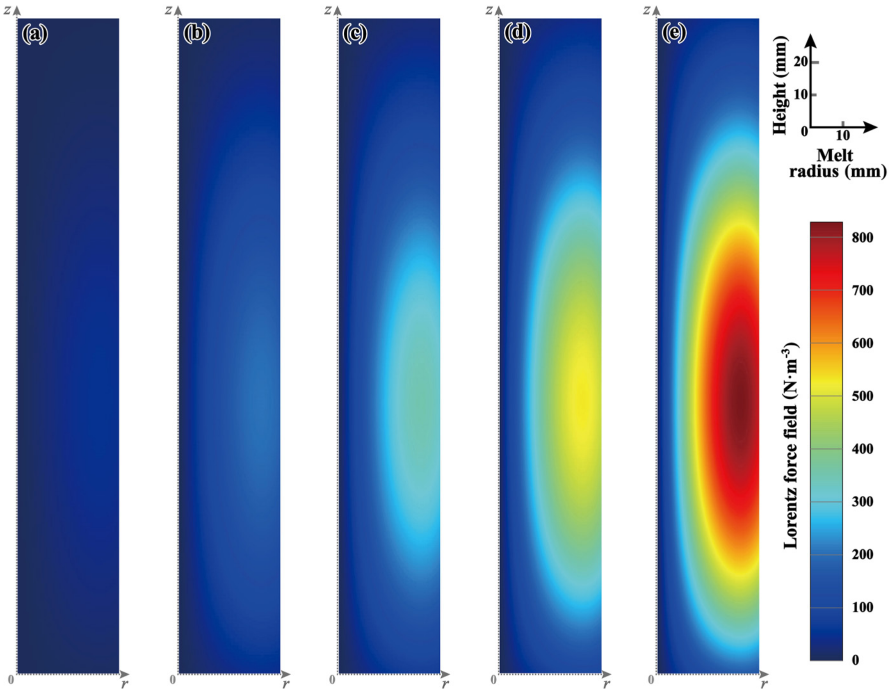

Fig. 5: Lorentz force field with different current frequencies: (a) 5 Hz; (b) 10 Hz; (c) 13 Hz; (d) 16 Hz; (e) 20 Hz

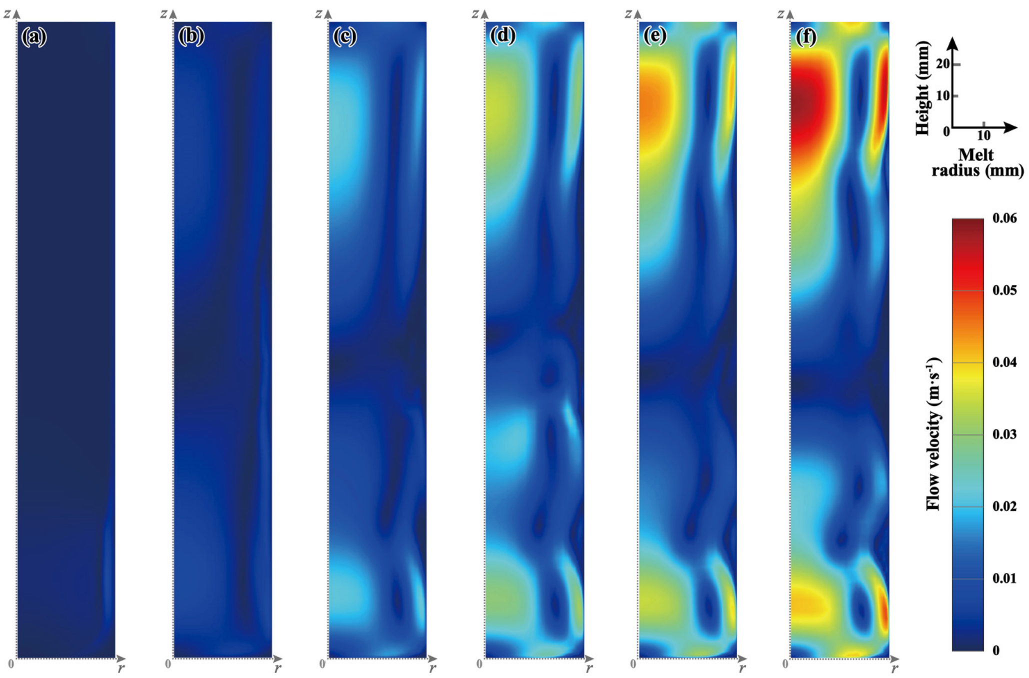

Fig. 6: Melt flow field with different current frequencies at 15 s: (a) without LFEC; (b) 5 Hz; (c) 10 Hz; (d) 13 Hz; (e) 16 Hz; (f) 20 Hz

that at the edge of the melt, and the melt velocity is higher in the upper part of the melt than that in the bottom part of the melt.

3.4 Temperature field

Figure 7 shows the temperature field of the melt with different current frequencies at 15 s. The temperature at the center is higher than that at the edge of the melt. With the application of LFEC, temperature field of the melt becomes more uniform with increasing the current frequency, thus the temperature gradient of the melt decreases, resulting in a lower superheat in the melt.

4 Discussion

4.1 Grain refinement mechanism

The above experimental results demonstrate that the grains can be refined and the CET can be promoted with the application of the low frequency electromagnetic field. During solidification, the grain size depends on the competition between the nucleation rate and grain growth rate. If the nucleation rate is higher than the growth rate, the grain will be refined.

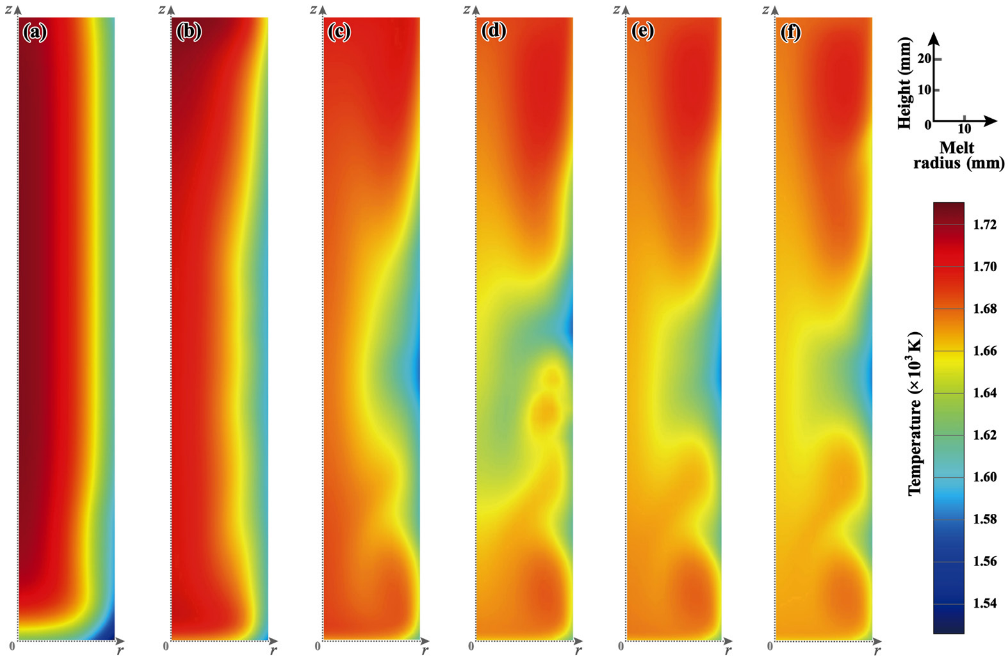

Fig. 7: Temperature field with different current frequencies at 15 s: (a) without LFEC; (b) 5 Hz; (c) 10 Hz; (d) 13 Hz; (e) 16 Hz; (f) 20 Hz

It is well known that heterogeneous nucleation is an effective method for grain refinement of alloys [27]. Under the low frequency electromagnetic field, a magnetic field is generated in the melt by the low frequency current, which creates an induced current in the melt. In this way, the melt is subjected to the Lorentz force generated from the interaction between the magnetic field and the induced current. During the solidification process, both the nucleation and growth of the grains are influenced by the Lorentz force. In the initial stage of the solidification, a multiplication of dendrites forms on the mold wall because of the high degree of undercooling between the melt and the mold wall. For the same material, the electrical resistivity in the solid is lower than that in the liquid [28]. The induced current generated by the low frequency electromagnetic field is higher in dendrites than that in the residual liquid. Thus, the dendrites are subjected to a larger Lorentz force. In this case, the initial solidified dendrites are favorable to be separated from the mold wall, which can act as the nucleation site for grains.

In addition, the average grain size decreases with increasing the current frequency. Although the depth of the Lorentz force decreases with increasing the current frequency because of the skin effect, the magnitude of the Lorentz force increases. The Lorentz force is mainly concentrated in the melt region near the mold wall, which is an important region for grain nucleation. Dendrites firstly form on the mold wall, and when the Lorentz force is greater than the strength of the dendrite root, dendrites detach from the mold wall, resulting in an increased heterogeneous nucleation in the melt. As more fragments form, the nucleation rate increases. The grain growth is confined by neighboring grains, leading to a grain refinement.

Furthermore, forced convection occurs, since the Lorentz force accelerates melt flow and heat transfer in the melt. Moreover, the melt flow plays an important role for grain refinement [29]. The melt flow is caused by both natural and forced convection. Without the low frequency electromagnetic field, there is only natural convection, so the melt flow velocity is slow [Fig. 6(a)]. As a result, only a small amount of dendrites detach from the mold wall, the grains are coarse. While, with the application of the low frequency electromagnetic field, forced convection is induced, which accelerates the melt flow velocity, as can be seen in Figs. 6(b–f). The interaction between forced melt flow and dendrites reduces the stability of dendrites growth [30], and breaks the dendrites, which promotes dendrite fragmentation.

Because of the forced melt flow generated by the electromagnetic field, the detachment of the dendrites from the mold wall can be transported to the undercooling region. New nuclei continue to form near the mold wall, thus more heterogeneous nucleation sites in the melt are effectively promoted. At the same time, the top free surface of the melt is fluctuated by the melt flow, and new nuclei are constantly formed and dispersed into the melt because of the low temperature of air, resulting in a larger number of nuclei in the melt. The forced melt flow increases with increasing current frequency, and the number of fragments at the solidification front increases, and thus more nucleation sites for equiaxed grains are promoted. If the number of nucleation sites for new grains is sufficiently large, the growth of grains is mutually limited, resulting in the refinement of equiaxed grains.

In fact, the temperature field is also influenced by the forced melt flow. The temperature distribution is more uniform under the electromagnetic field. It is well known that the grain size and morphology are influenced by the solidification conditions such as temperature gradient and cooling rate. The fine equiaxed grains easily form under the high cooling rates. On the one hand, with increasing the current frequency, the cooling rate increases, therefore, the undercooling in the melt also increases. More nuclei are promoted by a high cooling rate and results in grain refinement [31].

On the other hand, the superheat of the melt can affect the survival probability of the nuclei. When the current frequency is low, the forced convection is weak and the superheat in the melt center is high. If the fragments are transferred from mold wall (low temperature region) to the melt center (high temperature region), they may be remelted and cannot survive as nucleation sites for new grains. Therefore, nuclei survival is more favorable at the low superheat conditions. As a result, the probability of remelting of dendrite fragments is reduced with a lower temperature gradient [32]. The high undercooling and low temperature gradient are favorable for the formation of fine grains [33].

In addition, applied electromagnetic field can change the Gibbs free energy ΔG, which can be expressed as [34,35]:

$$\Delta G = \Delta G_{\mathrm{v}} + \Delta G_{\mathrm{m}} \tag{12}$$

where the ΔG_{v} is the difference between the free energy of the solid phase and the liquid phase per unit volume. The ΔG_{m} is the change in magnetic free energy formed per unit volume of the solid phase, which can be written as:

$$\Delta G_{\mathrm{m}} = -\frac{\chi^{\mathrm{ls}}\boldsymbol{B}^2}{2\mu_0} - \frac{\boldsymbol{B}^2}{2\mu_0} \tag{13}$$

where the χ^{ls} is the change of volume susceptibility between the solid phase and the liquid phase, and μ_0 is the magnetic permeability.

The total free energy change ΔG_{T} can be described as:

$$\Delta G_{\mathrm{T}} = \left(\frac{4}{3}\pi r^3 \Delta G + 4\pi r^2 \sigma_{\alpha \mathrm{l}}\right)\left(\frac{2 - 3\cos\theta + \cos^3\theta}{4}\right) \tag{14}$$

where the $\sigma_{\alpha \mathrm{l}}$ is the interfacial tension between the solid phase and liquid phase.

Therefore, the critical nucleation energy ΔG_{T}^* is obtained as follows:

$$\Delta G_{\mathrm{T}}^* = \frac{16\pi\sigma_{\alpha \mathrm{l}}^3}{3\left[\Delta G_{\mathrm{V}} + \left(-\chi^{\mathrm{ls}}\boldsymbol{B}^2 - \boldsymbol{B}^2\right)/2\mu_0\right]^2} \times \left(\frac{2 - 3\cos\theta + \cos^3\theta}{4}\right) \tag{15}$$

The critical nucleation radius r^* can be obtained as follows:

$$r^* = \frac{-2\sigma_{\alpha \mathrm{l}}}{\left(\Delta G_{\mathrm{V}} + \left(-\chi^{\mathrm{ls}}\boldsymbol{B}^2 - \boldsymbol{B}^2\right)/2\mu_0\right)} \tag{16}$$

It can be concluded that with the application of the low frequency electromagnetic field, the energy barrier and critical radius of nucleation can be reduced. Therefore, the nucleation rate is increased by the low frequency electromagnetic field and the grain size is reduced through changing of both the melt flow field (as shown in Fig. 6) and temperature field (as shown in Fig. 7).

4.2 CET mechanism

The transition process of macrostructure from columnar grains to equiaxed grains during solidification is called CET [36]. The CET occurs when the growth of columnar grains is hindered by the formation of new equiaxed grains [37]. In fact, an equiaxed zone forms when the nucleation rate for equiaxed grains is sufficiently large to obstruct the growth of columnar grains. Therefore, the CET depends on the competitive growth of the columnar grains and equiaxed grains. Another fact is that the columnar and equiaxed grains on both sides of the CET boundary are interdependent in scale. Nucleation sites for equiaxed grains can be provided by the fragmented dendrites [38]. Under magnetic field, fragmentation is caused by the action of force field and the CET is promoted [39]. The high nucleation rate in the solidification front resulting in the formation of equiaxed grains [40]. More nuclei can be generated by the melt flow from the mold wall and melt top surface. They are transported to the undercooled region in the front of the columnar grains, and eventually equiaxed grains form. In the present study, both the temperature field (Fig. 7) and melt flow field (Fig. 6) are changed with the application of the electromagnetic field during the solidification process of the alloy. The fragmentation or remelting of the dendrites is intensified and the solidification nucleation rate is increased, resulting in grain refinement [Fig. 4(a)] and the promotion of CET [Fig. 4(b)].

4.3 Simulation for the large size VIM ingot

Large size GH4742 superalloy VIM ingot is prone to form hot cracking, but the cost of full-size experiment is too high. Therefore, based on the results of the present study, the way for inhibiting the hot cracking tendency of the large size GH4742 superalloy VIM ingot is explored with numerical simulation.

According to the above experimental and numerical simulation results, it can be seen that the grains can be effectively refined and the CET is promoted through applying a low frequency electromagnetic field during the solidification process of GH4742 superalloy. Based on the statistical data of large size electrodes cracking in the industrial production and the results of previous studies [41], it has been found that the coarse dendrites in the coarse columnar grains of tens of millimetres and more than half of the coarse dendrites in the columnar grains, while the columnar grains and equiaxed grains on both sides of CET are interdependent in scale. The excessive segregation of alloying elements in dendrites is the root cause of electrode cracking [3]. Then, for large size VIM electrodes, the same numerical simulation method as above was used for prediction. The numerical simulation of ingots with the diameter of 60 mm to 430 mm, was based on the following conditions:

(1) CET ratio of VIM electrode must be higher than 50%;

(2) The electrode cracking sensitive temperature (solid fraction is 0.9 [42]) must be in the equiaxed grain zone near the CET;

(3) The current frequency was set to 5 Hz (considering the depth of action), with current densities of 100 A, 200 A, 300 A, and 400 A, respectively.

According to the above conditions, the numerical simulation results are shown in Figs. 8 and 9. Figure 8 shows the temperature field of the 60 mm diameter ingot melt with different current frequencies when the solid fraction of Point A (22, 100) is 0.9. It can be seen that the temperature gradient is the largest in the melt without LFEC. With the application of LFEC, temperature field of the melt becomes more uniform. In addition, with increasing the current frequency, the temperature gradient decreases. When the current frequency reaches 20 Hz,

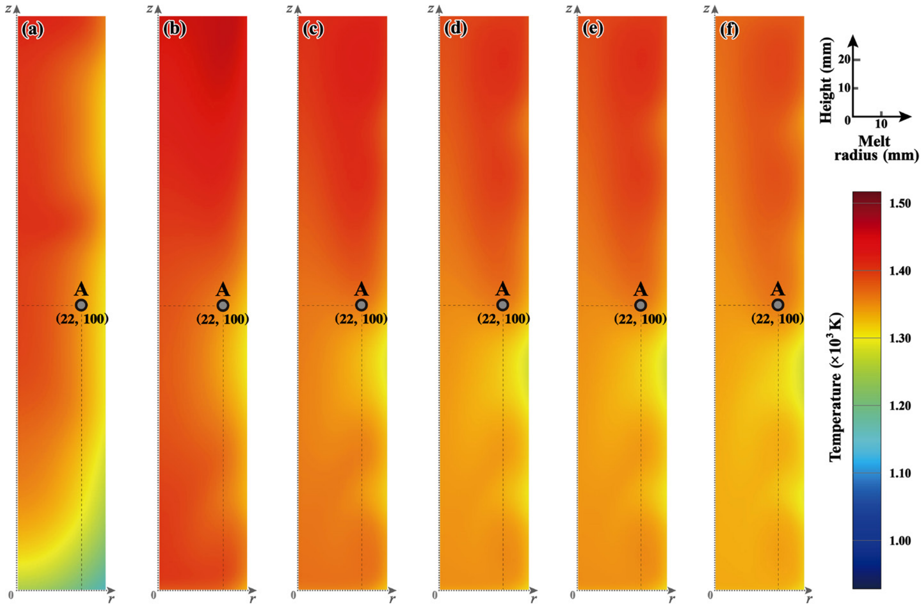

Fig. 8: Temperature field of 60 mm diameter ingot with different current frequencies: (a) without LFEC; (b) 5 Hz; (c) 10 Hz; (d) 13 Hz; (e) 16 Hz; (f) 20 Hz

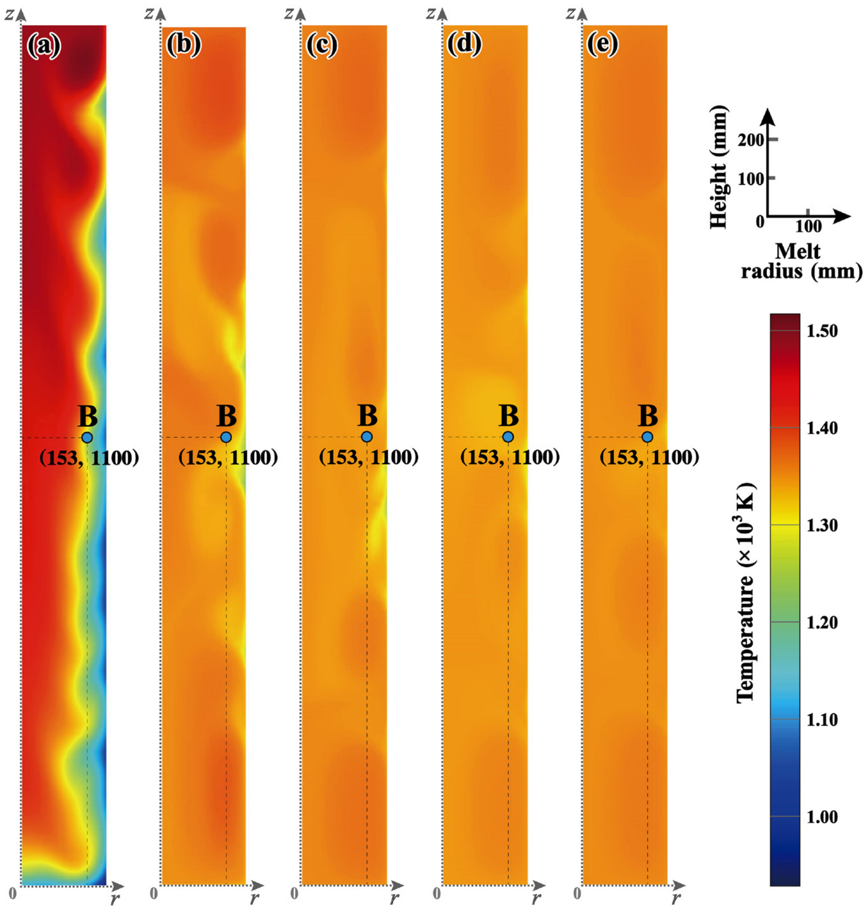

Fig. 9: Temperature field of 430 mm diameter electrode with different current densities: (a) without LFEC; (b) 100 A; (c) 200 A; (d) 300 A; (e) 400 A

the temperature field is the most uniform. Figure 9 shows the temperature field of 430 mm diameter electrode melt with different current densities when the solid fraction of Point B (153, 1100) is 0.9. Due to the increase in the melt size, the temperature field of the melt without LFEC is extreme uneven. The temperature in the melt center is very high, and the temperature near the melt edge is very low. Therefore, a large temperature gradient forms in the melt. With the application of LFEC, the temperature becomes uniform. In addition, with increasing the current density, the temperature field becomes more uniform. When the current density reaches 400 A, the temperature field is the most uniform, and the temperature gradient is the lowest. Comparing the results shown in Fig. 8 with that in Fig. 9, it is clear that with the application of the low frequency electromagnetic field of 400 A and 5 Hz, no less than 50% CET can be obtained for the VIM electrode with a diameter of 430 mm, since the temperature field cloud image is similar to the result of the 60 mm diameter ingot, as shown in Fig. 8. It is suggested that when the LFEC parameters can be effectively controlled during the preparation of GH4742 superalloy with a diameter of 430 mm VIM electrode, coarse dendrites with a high degree of segregation would not form, and the cracking of VIM electrode can also be inhibited.

5 Conclusions

(1) With the application of the low frequency electromagnetic fields, the average grain size is reduced and CET is promoted for the GH4742 superalloy ingot. In addition, the average equiaxed grain size decreases and the fraction of equiaxed grains increases with increasing the current frequency.

(2) With the application of the low frequency electromagnetic fields, the forced convection occurs due to the Lorentz force, and the melt flow velocity increases. In this way, more nuclei are generated in the melt, resulting in finer grains.

(3) The temperature field becomes more uniform and the superheat is lower with low frequency electromagnetic fields, which is a favorable condition for the survival of nuclei.

(4) Based on the results of experiments and numerical simulation, it is found that the forced melt flow generated by Lorentz force can effectively refine grains and promote CET. It indicates that the hot cracking of the large size GH4742 superalloy VIM electrodes can be prevented through applying a low frequency electromagnetic field with proper parameters.

Acknowledgments

This research work was financially supported by the Major Projects in Aviation Engines and Gas Turbines (Grant No. 2019-VI-0020-0136), the National Key Research and Development Program of China (Grant Nos. 2022YFB3705101 & 2022YFB3705102), the National Natural Science Foundation of China (Grant No. U1708253), and the Fundamental Research Funds for the Central Universities, China (Grant No. N2302005).

Conflict of interest

The authors declare that they have no known competing financial interests or personal relationships that could have appeared to influence the work reported in this paper.

References

[1] Lu X D, Deng Q, Du J H, et al. Effect of slow cooling treatment on microstructure of difficult deformation GH4742 superalloy. Journal of Alloys and Compounds, 2009, 477(1): 100–103. https://doi.org/10.1016/j.jallcom.2008.10.088

[2] Kong W W, Yuan C, Zhang B N. Investigations on cyclic deformation behaviors and corresponding failure modes of a Ni-based superalloy. Materials Science and Engineering: A, 2020, 791: 139775. https://doi.org/10.1016/j.msea.2020.139775

[3] Zhang L, Wang L, Liu Y, et al. Hot cracking behavior of large size GH4742 superalloy vacuum induction melting ingot. Journal of Iron and Steel Research International, 2022, 29(9): 1505–1512. https://doi.org/10.1007/s42243-022-00767-7

[4] Bai Q L, Li Y, Li H X, et al. Roles of alloy composition and grain refinement on hot tearing susceptibility of 7xxx aluminum alloys. Metallurgical and Materials Transactions: A, 2016, 47(8): 4080–4091. https://doi.org/10.1007/s11661-016-3588-2

[5] Qin H, Yang G Y, Zheng X W, et al. Effect of Gd content on hot-tearing susceptibility of Mg-6Zn-*x*Gd casting alloys. China Foundry, 2022, 19(2): 131–139. https://doi.org/10.1007/s41230-022-1117-z

[6] Li S, Sadayappan K, Apelian D. Role of grain refinement in the hot tearing of cast Al-Cu alloy. Metallurgical and Materials Transactions: B, 2013, 44(3): 614–623. https://doi.org/10.1007/s11663-013-9801-4

[7] Lin S, Aliravci C, Pekguleryuz M O. Hot-tear susceptibility of aluminum wrought alloys and the effect of grain refining. Metallurgical and Materials Transactions: A, 2007, 38(5): 1056–1068. https://doi.org/10.1007/s11661-007-9132-7

[8] Zhang Y H, Ye C Y, Shen Y P, et al. Grain refinement of hypoeutectic Al-7wt.%Si alloy induced by an Al-V-B master alloy. Journal of Alloys and Compounds, 2020, 812: 152022. https://doi.org/10.1016/j.jallcom.2019.152022

[9] Metan V, Eigenfeld K, Räbiger D, et al. Grain size control in Al-Si alloys by grain refinement and electromagnetic stirring. Journal of Alloys and Compounds, 2009, 487(1): 163–172. https://doi.org/10.1016/j.jallcom.2009.08.032

[10] Fan S, Wu H B, Fang J X. Microstructure and mechanical properties of AZ91D magnesium alloy by expendable pattern shell casting with different mechanical vibration amplitudes and pouring temperatures. China Foundry, 2021, 18(1): 1–8. https://doi.org/10.1007/s41230-021-0113-z

[11] Taghavi F, Saghafian H, Kharrazi Y H K. Study on the effect of prolonged mechanical vibration on the grain refinement and density of A356 aluminum alloy. Materials & Design, 2009, 30(5): 1604–1611. https://doi.org/10.1016/j.matdes.2008.07.032

[12] Wang X, Hu Y J, Wang J Y, et al. Microstructure evolution and mechanical property of quaternary Cu-7%Al-4%Ni-2.5%Mn alloy solidified within ultrasonic field. Journal of Alloys and Compounds, 2021, 881: 160604. https://doi.org/10.1016/j.jallcom.2021.160604

[13] Zhang S R, Kang H J, Cheng M, et al. Ultrasound-assisted solidification of a Cu-Cr alloy. Acta Metallurgica Sinica (English Letters), 2022, 35(12): 2082–2088. https://doi.org/10.1007/s40195-022-01433-3

[14] Yan W, Chen W Q, Zhang S L, et al. Evolution of solidification structures and mechanical properties of high-Si Al alloys under permanent magnetic stirring. Materials Characterization, 2019, 157: 109894. https://doi.org/10.1016/j.matchar.2019.109894

[15] Zeng J, Song L L, Peng J F, et al. Experimental study and numerical simulation of permanent magnet stirring on solidification of IN718 superalloy under different rotation speeds. Journal of Alloys and Compounds, 2023, 954: 170223. https://doi.org/10.1016/j.jallcom.2023.170223

[16] Dai K, Ye J Y, Wang Z G, et al. Beneficial utilization of electromagnetic stirring technology in Al-Ce alloys. JOM, 2023, 75(8): 2788–2798. https://doi.org/10.1007/s11837-023-05904-5

[17] Nafisi S, Emadi D, Shehata M T, et al. Effects of electromagnetic stirring and superheat on the microstructural characteristics of Al-Si-Fe alloy. Materials Science and Engineering: A, 2006, 432(1): 71–83. https://doi.org/10.1016/j.msea.2006.05.076

[18] Wang F Y, Wang N, Yu F, et al. Study on micro-structure, solid solubility and tensile properties of 5A90 Al-Li alloy cast by low-frequency electromagnetic casting processing. Journal of Alloys and Compounds, 2020, 820: 153318. https://doi.org/10.1016/j.jallcom.2019.153318

[19] Wang F Y, Wang X J, Sun W, et al. Low frequency electromagnetic casting of 2195 aluminum-lithium alloy and its effects on microstructure and mechanical properties. Acta Metallurgica Sinica (English Letters), 2020, 33(3): 338–350. https://doi.org/10.1007/s40195-019-00992-2

[20] Zuo Y B, Cui J Z, Zhao Z H, et al. Mechanism of grain refinement of an Al-Zn-Mg-Cu alloy prepared by low-frequency electromagnetic casting. Journal of Materials Science, 2012, 47(14): 5501–5508. https://doi.org/10.1007/s10853-012-6441-z

[21] Wang Y X, Zeng X Q, Ding W J, et al. Grain refinement of AZ31 magnesium alloy by titanium and low-frequency electromagnetic casting. Metallurgical and Materials Transactions: A, 2007, 38(6): 1358–1366. https://doi.org/10.1007/s11661-007-9215-5

[22] Zhang H T, Nagaumi H, Zuo Y B, et al. Coupled modeling of electromagnetic field, fluid flow, heat transfer and solidification during low frequency electromagnetic casting of 7XXX aluminum alloys: Part 1: Development of a mathematical model and comparison with experimental results. Materials Science and Engineering: A, 2007, 448(1): 189–203. https://doi.org/10.1016/j.msea.2006.10.062

[23] Zou J, Zhang H T, Wu Z B, et al. Effects of an intermittent permanent magnet stirring on the melt flow and grain refinement of Al-4.5Cu alloy. Journal of Materials Research and Technology, 2021, 14: 1585–1600. https://doi.org/10.1016/j.jmrt.2021.07.039

[24] Brent A D, Voller V R, Reid K J. Enthalpy-porosity technique for modeling convection-diffusion phase change: Application to the melting of a pure metal. Numerical Heat Transfer, 1988, 13(3): 297–318. https://doi.org/10.1080/10407788808913615

[25] Wang J H, Wang L, Song X, et al. Effects of permanent magnetic stirring on the solidification nucleation behavior of GH4742 superalloy. JOM, 2023, 75(8): 2818–2827. https://doi.org/10.1007/s11837-023-05740-7

[26] Jia Y H, Zou Q, Chen X R, et al. Study on heat transfer behavior and process optimization in differential phase electromagnetic DC casting of extra-large AZ31B alloy flat ingot: Numerical simulation and experimental verification. Journal of Materials Research and Technology, 2023, 24: 1108–1131. https://doi.org/10.1016/j.jmrt.2023.03.014

[27] Liu X W, Laplanche G, Kostka A, et al. Columnar to equiaxed transition and grain refinement of cast CrCoNi medium-entropy alloy by microalloying with titanium and carbon. Journal of Alloys and Compounds, 2019, 775: 1068–1076. https://doi.org/10.1016/j.jallcom.2018.10.187

[28] Zhou Y, Mao P L, Wang Z, et al. Effect of low frequency alternating magnetic field on hot tearing susceptibility of Mg-7Zn-1Cu-0.6Zr magnesium alloy. Journal of Materials Processing Technology, 2020, 282: 116679. https://doi.org/10.1016/j.jmatprotec.2020.116679

[29] Jie J C, Yue S P, Liu J, et al. Revealing the mechanisms for the nucleation and formation of equiaxed grains in commercial purity aluminum by fluid-solid coupling induced by a pulsed magnetic field. Acta Materialia, 2021, 208: 116747. https://doi.org/10.1016/j.actamat.2021.116747

[30] Zhang K L, Li Y J, Yang Y S. Influence of the low voltage pulsed magnetic field on the columnar-to-equiaxed transition during directional solidification of superalloy K4169. Journal of Materials Science & Technology, 2020, 48: 9–17. https://doi.org/10.1016/j.jmst.2020.02.009

[31] Shao Z W, Le Q C, Zhang Z Q, et al. A new method of semi-continuous casting of AZ80 Mg alloy billets by a combination of electromagnetic and ultrasonic fields. Materials & Design, 2011, 32(8): 4216–4224. https://doi.org/10.1016/j.matdes.2011.04.035

[32] Griffiths W D, Mccartney D G. The effect of electromagnetic stirring during solidification on the structure of Al-Si alloys. Materials Science and Engineering: A, 1996, 216(1): 47–60. https://doi.org/10.1016/0921-5093(96)10392-0

[33] Campanella T, Charbon C, Rappaz M. Influence of permeability on the grain refinement induced by forced convection in copper-base alloys. Scripta Materialia, 2003, 49(10): 1029–1034. https://doi.org/10.1016/S1359-6462(03)00446-9

[34] Li Y J, Tao W Z, Yang Y S. Grain refinement of Al-Cu alloy in low voltage pulsed magnetic field. Journal of Materials Processing Technology, 2012, 212(4): 903–909. https://doi.org/10.1016/j.jmatprotec.2011.11.018

[35] Duan W C, Yin S Q, Liu W H, et al. Numerical and experimental studies on solidification of AZ80 magnesium alloy under out-of-phase pulsed magnetic field. Journal of Magnesium and Alloys, 2021, 9(1): 166–182. https://doi.org/10.1016/j.jma.2020.03.008

[36] Biscuola V B, Martorano M A. Mechanical blocking mechanism for the columnar to equiaxed transition. Metallurgical and Materials Transactions: A, 2008, 39(12): 2885–2895. https://doi.org/10.1007/s11661-008-9643-x

[37] Martorano M A, Beckermann C, Gandin C A. A solutal interaction mechanism for the columnar-to-equiaxed transition in alloy solidification. Metallurgical and Materials Transactions: A, 2003, 34(8): 1657–1674. https://doi.org/10.1007/s11661-003-0311-x

[38] Agrawal S, Ghose A K, Chakrabarty I. Effect of rotary electromagnetic stirring during solidification of in-situ Al-TiB_2 composites. Materials & Design, 2017, 113: 195-206. https://doi.org/10.1016/j.matdes.2016.10.007

[39] Li X, Gagnoud A, Fautrelle Y, et al. Dendrite fragmentation and columnar-to-equiaxed transition during directional solidification at lower growth speed under a strong magnetic field. Acta Materialia, 2012, 60(8): 3321–3332. https://doi.org/10.1016/j.actamat.2012.02.019

[40] Yue X A, Shen J, Wang L, et al. Microstructure evolution and mechanical properties of directionally solidified large size Ti-47Al-5Nb-0.18C-0.3Si alloy by electromagnetic confinement. Journal of Alloys and Compounds, 2022, 891: 161762. https://doi.org/10.1016/j.jallcom.2021.161762

[41] Li Q. Study on electrode cracking behavior of nickel-base superalloy by vacuum induction furnace melting. Masters' Dissertation, Shenyang: Northeastern University, 2017. https://doi.org/10.27007/d.cnki.gdbeu.2018.002522 (In Chinese)

[42] Eskin D G, Suyitno, Katgerman L. Mechanical properties in the semi-solid state and hot tearing of aluminium alloys. Progress in Materials Science, 2004, 49(5): 629–711. https://doi.org/10.1016/S0079-6425(03)00037-9